1 Introduction

Since 1967, the Nuclear Regulatory Commission (NRC) and its predecessor the Atomic Energy Commission (AEC) have conducted research programs that address aging of reactor components. The results of this research have been used to evaluate and establish regulatory guidelines to ensure acceptable levels of reliability for light water reactor (LWR) components. The products of this program, i.e., technical reports, methodologies for evaluating licensee submittals, and other inputs to the regulatory process, have led to the resolution of regulatory issues, as well as the development, validation, and improvement of regulations and regulatory guides. The research on the effects of the environment on component cracking was initiated in response to the determination that environmental effects were critical to several important cracking phenomena in LWR components. A major research program at Argonne National Laboratory (ANL) was initiated in 1979 to address pipe–cracking problems in boiling water reactors (BWRs). Since that time, in response to needs for additional research to support the Office of Nuclear Reactor Regulation (NRR) to assess developing cracking problems in aging reactors, the focus of the project has shifted to address other problems in environmental cracking of LWR components. In recent years this activity has been supplemented by NRC participation in the programs associated with the International Cooperative Group on Environmentally Assisted Cracking (ICG–EAC), Halden reactor Project, and Cooperative Irradiation Assisted Stress Corrosion Cracking Research (CIR), all proprietary activities in which groups in several countries contribute money that is used to support research on environmentally assisted cracking (EAC) problems of common interest.

This project consists of several tasks with differing objectives; so the objectives are best described on a task–by–task basis:

Task 1: Environmental Effects on Fatigue Crack Initiation.

The objective of this task is to provide information on such topics as fatigue crack initiation in stainless steel (SS), and the synergistic effects of surface finish or loading sequence and environment on fatigue life. A comprehensive evaluation of SS fatigue test specimens will be performed to explain why environmental effects are more pronounced in low–dissolved oxygen (DO) than high–DO water. The contractor will review and evaluate issues related to environmental effects on fatigue as required by the NRC, and will participate in ASME Code committees to incorporate the effects of LWR environments in fatigue life analyses.

Task 2: Evaluation of the Causes and Mechanisms of IASCC in BWRs.

This task will evaluate the susceptibility of austenitic SSs, their welds, and selected Ni–base alloys to IASCC as a function of fluence level, water chemistry, material chemistry, welding process, and fabrication history. It will provide data and technical support required for determination of inspection intervals. The purpose is to help NRC address various issues that arise in license renewal or other licensee submittals. Crack growth rate (CGR) tests and slow strain rate tests (SSRTs) will be conducted on high–fluence model SSs from Halden Phase–I irradiations (carried out under NRC FIN W6610) to investigate the effects of material chemistry and irradiation level on the susceptibility of SSs to IASCC. CGR tests will be conducted on submerged arc (SA) and shielded metal arc (SMA) welds of Type 304 and 304L steels irradiated to 1.2×10^{21} n/cm^2 (1.8 dpa) in the Halden reactor to establish the effects of fluence level, material chemistry, and welding process on IASCC. Also, SSRTs and CGR tests will be carried out on grain boundary optimized (GBO) model SS alloys to study the effect of grain boundary

geometry on IASCC and assess the prospect of using GBO as a mitigative measure. Models and codes developed under CIR and from industry sources will be benchmarked and used in conjunction with this work.

Industry-developed crack growth models will be analyzed and assessed. Also, the effectiveness of mitigative water chemistry measures, e.g., hydrogen water chemistry or noble metal additions, will be assessed. Much of this assessment will depend on data provided by industry, data available in the literature, and developed as part of this task. However, for CGR models for irradiated materials, it is anticipated that relatively few data will be available because of the expense and difficulty of testing. Additional testing on nonirradiated materials will be performed to provide "limiting cases" against which the models can be tested. These tests will seek to determine the effects of Cr level in the steel and cold work on CGRs in austenitic SSs in LWR environments. This will be accomplished by procuring material and fabricating and testing compact–tension (CT) specimens from model SS alloys with low Cr content and cold–worked (CW) Type 304L and 304 SS.

Task 3: Evaluation of Causes and Mechanisms of IASCC of Austenitic SS in PWRs.

The task will evaluate (a) the effects of very high fluence on CGRs, (b) neutron irradiation embrittlement, e.g., loss of fracture toughness, and (c) void swelling behavior in austenitic SSs. Tests will be conducted on material procured from the EBR–II reactor hexagonal fuel channels or irradiated in the BOR–60 reactor in Russia and shipped to Argonne.

Task 4: Cracking of Nickel Alloys and Weldments.

The objective of this task is to provide the NRC with technical data on the implications of cracks in Ni–alloy components and weldments for residual life, inspection, and repair. Many reactor vessel internal components and their attachment welds, vessel penetrations, and piping butt welds are made of alloys such as Alloy 600 or 690, Alloy X750, and Alloy 182 or 152, which are susceptible to intergranular stress corrosion cracking (IGSCC). The causes and mechanisms of this cracking and the implications of microstructure, microchemistry, and surface finish for component life are also not well understood, and thus lead to greater uncertainty in licensee submissions that address issues such as damage accumulation and inspection intervals. The NRC research program will address these issues and provide data required to support staff assessment of industry CGR models, and potential crack detection and mitigation measures.

Task 5: Investigation of Other Modes of Degradation in High–Fluence Materials in PWR Environments.

This task will focus on developing technical letter reports on various aspects of the degradation of high–dose (>10 dpa) reactor internals in PWR environments, e.g., issues of void swelling, stress corrosion cracking, and the possible synergistic effects of thermal and radiation embrittlement of cast and wrought stainless steels. The contents of these reports shall be drawn from available literature, the products of past and on–going industry or DOE programs, and the background of the authors of these reports.

2 Environmental Effects on Fatigue Crack Initiation in Carbon and Low–Alloy Steels and Austenitic Stainless Steels (O. K. Chopra and B. Alexandreanu)

2.1 Introduction

Cyclic loadings on a structural component occur because of changes in mechanical and thermal loadings as the system goes from one load set (e.g., pressure, temperature, moment, and force loading) to any other load set. For each load set, an individual fatigue usage factor is determined by the ratio of the number of cycles anticipated during the lifetime of the component to the allowable cycles. Figures I–9.1 through I–9.6 of Appendix I to Section III of the ASME Boiler and Pressure Vessel Code specify fatigue design curves that define the allowable number of cycles as a function of applied stress amplitude. The cumulative usage factor (CUF) is the sum of the individual usage factors, and the ASME Code Section III requires that the CUF at each location must not exceed 1.

The ASME Code fatigue design curves, given in Appendix I of Section III, are based on strain–controlled tests of small polished specimens at room temperature in air. The design curves have been developed from the best–fit curves to the experimental fatigue–strain–vs.–life (ε–N) data that are expressed in terms of the Langer equation[1] of the form

$$\varepsilon_a = A1(N)^{-n1} + A2, \tag{1}$$

where ε_a is the applied strain amplitude, N is the fatigue life, and A1, A2, and n1 are coefficients of the model. Equation 1 may be written in terms of stress amplitude S_a instead of ε_a, in which case stress amplitude is the product of ε_a and elastic modulus E, i.e., $S_a = E\,\varepsilon_a$. The fatigue design curves were obtained from the best–fit curves by first adjusting for the effects of mean stress on fatigue life and then reducing the fatigue life at each point on the adjusted curve by a factor of 2 on strain (or stress) or 20 on cycles, whichever is more conservative.

The factors of 2 and 20 are not safety margins but rather conversion factors that must be applied to the experimental data to obtain reasonable estimates of the lives of actual reactor components. Although the Section III criteria document[2] states that these factors were intended to cover such effects as environment, size, and scatter of data, Subsection NB–3121 of Section III of the Code explicitly notes that the data used to develop the fatigue design curves (Figs. I–9.1 through I–9.6 of Appendix I to Section III) did not include tests in the presence of corrosive environments that might accelerate fatigue failure. Article B–2131 in Appendix B to Section III states that the owner's design specifications should provide information about any reduction to fatigue design curves that has been necessitated by environmental conditions.

The existing fatigue ε–N data illustrate potentially significant effects of light water reactor (LWR) coolant environments on the fatigue resistance of carbon and low–alloy steels,[3–5] as well as austenitic stainless steels (SSs).[4–7] Under certain environmental and loading conditions, fatigue lives of austenitic SSs can be a factor of 20 lower in water than in air.[6]

In LWR environments, the fatigue lives of austenitic SSs depend on applied strain amplitude, strain rate, temperature, and dissolved oxygen (DO) in water. A minimum threshold strain is required for inducing an environmentally assisted decrease in the fatigue life.[7] Environmental effects on life occur primarily during the tensile–loading cycle and at strain levels greater than the threshold value. Strain rate

and temperature have a strong effect on fatigue life in LWR environments.[6,7] Fatigue life decreases logarithmically with decreasing strain rate below 0.4%/s; this effect vanishes at 0.0004%/s. In addition, the fatigue ε–N data suggest a threshold temperature of 150°C; in the range of 150–325°C, the logarithm of life decreases linearly with temperature. The effect of DO on fatigue life may depend on the composition and heat treatment of the steel. Limited data indicate that, in high–DO water, the environmental effects are influenced by the material heat treatment.[7] In low–DO water, the material heat treatment seems to have little or no effect on the fatigue life of austenitic SSs.

This section presents experimental data on the effect of heat treatment on fatigue crack initiation in austenitic SS in LWR coolant environments. Fatigue tests have been conducted on two heats of Type 304 SS under various conditions to determine the effect of heat treatment on fatigue crack initiation in these steels in air and LWR environments. A detailed metallographic examination of the fatigue test specimens was performed to characterize the crack morphology and fracture morphology in austenitic SSs in air, as well as BWR and PWR environments.

2.2 Experimental

Fatigue tests have been conducted on two heats of Type 304 SS in the mill–annealed (MA) as well as MA plus additional heat treatment conditions. The chemical compositions of the heats are given in Table 1. Heat 10285 was heat treated at 600°C for 24 h whereas two heat treatments were used for Heat 30956: 0.67 h at 700°C and 24 h at 700°C. These heat treatments correspond to EPR (electrochemical potentiodynamic reactivation) values of ≈16 C/cm^2 for Heat 10285,[8] and ≈8 and 30 C/cm^2, respectively, for Heat 30956.[9]

Table 1. Composition (wt.%) of austenitic stainless steels for fatigue tests.

Material	Source	C	P	S	Si	Cr	Ni	Mn	Mo
Type 304[a]	Supplier	0.060	0.019	0.007	0.48	18.99	8.00	1.54	0.44
Type 304[b]	Supplier	0.060	0.025	0.011	0.59	18.31	8.51	1.58	0.38

[a]76 x 25 mm bar stock, Heat 30956. Solution annealed at 1050°C for 0.5 h.
[b]25–mm–thick plate, Heat 10285. Solution annealed at 1050°C for 0.5 h.

The metallographic examination of the sensitized alloys was carried out on 10 x 10 x 10–mm specimens that were ground and polished with SiC paper by successively increasing the grade of the paper up to #4000, then finishing with 1–μm diamond paste. Next, the samples were electrochemically etched in a solution of HNO_3 (10%) and distilled water at 8 V for ≈15 s. The microstructure was examined by scanning electron microscopy (SEM) in a JEOL JSM–6400 microscope.

Typical photomicrographs obtained from the sensitized alloys are shown in Fig. 1. Etching revealed a partially sensitized microstructure for the MA Heat 30956 that was heat treated for 0.67 h at 700°C. This is most evident in the higher–magnification photomicrograph (Fig. 1b) showing that sensitization occurred selectively, most likely at curved, high–energy boundaries. A somewhat more uniform degree of sensitization was observed in MA Heat 10285 (heat–treated for 24 h at 600°C), where almost all non-twin boundaries were sensitized. Stringers, also observed in this heat, most likely were parts of the microstructure before the sensitization treatment. Sensitization of Heat 30956 for 24 h at 700°C affected all of the boundaries, especially the curved, high–energy ones; also, it appears that some incoherent twin boundaries were also affected (Fig. 1f).

Heat 30956, mill annealed plus heat treated 0.67 h at 700°C

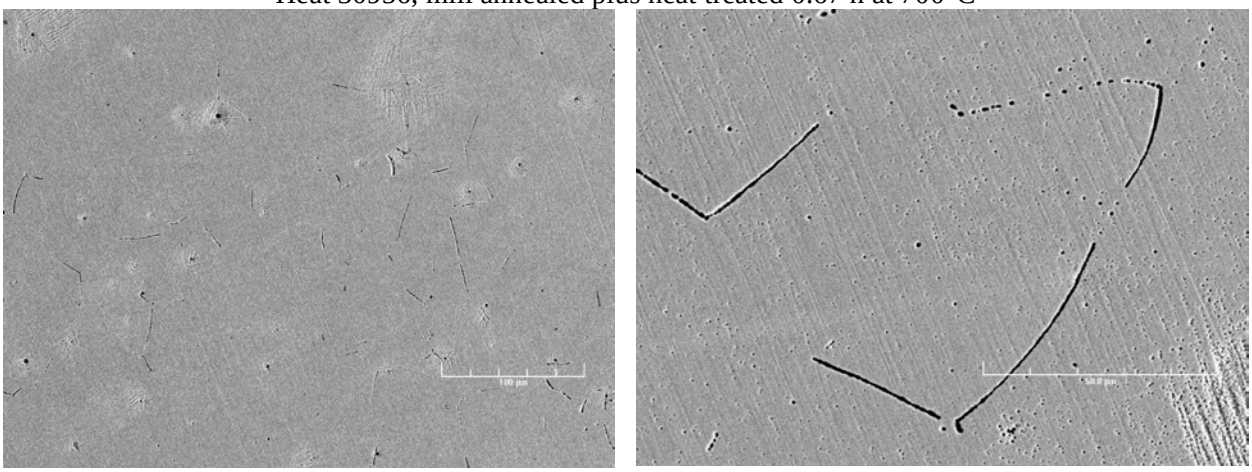

(a) (b)

Heat 10285, mill annealed plus heat treated 24 h at 600°C

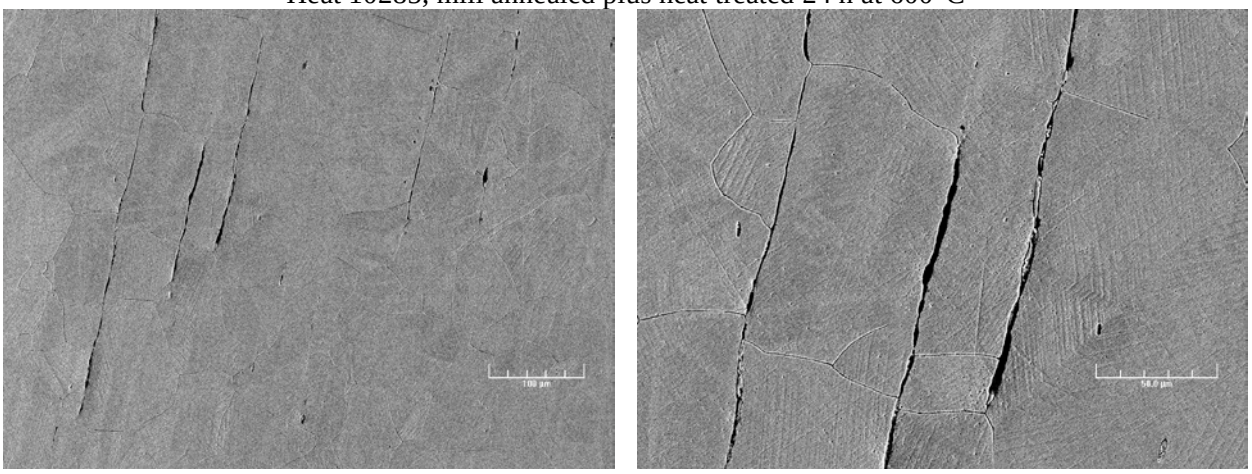

(c) (d)

Heat 30956, mill annealed plus heat treated 24 h at 700°C

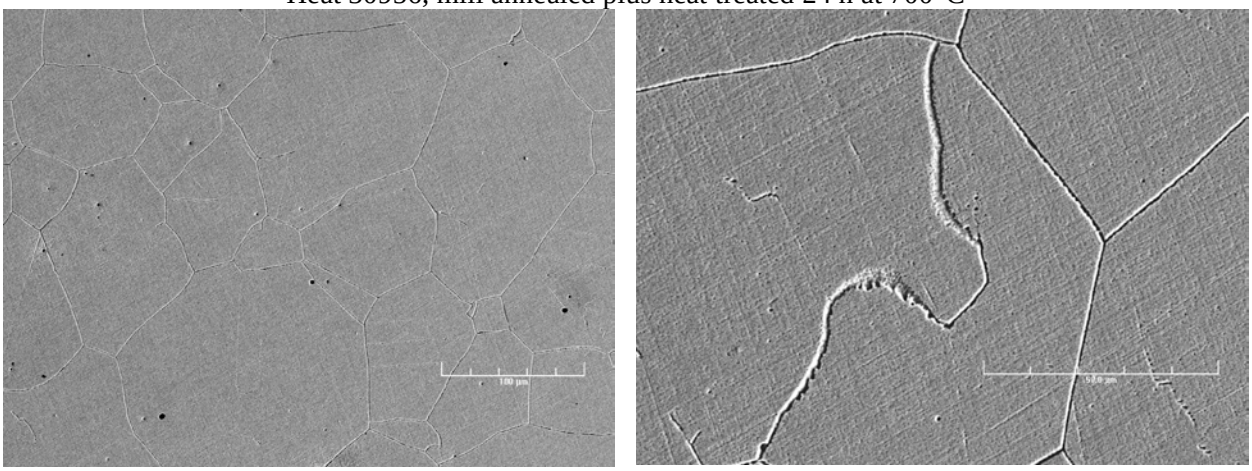

(e) (f)

Figure 1. Typical microstructures observed by SEM, showing degree of sensitization for alloys used in this study: (a), (c), (e), low magnification; (b), (d), (f), high magnification.

Smooth cylindrical specimens, with a 9.5–mm diameter and a 19–mm gauge length, were used for the fatigue tests (Fig. 2). The test specimens were machined from a composite bar fabricated by electron–beam welding of two 19.8–mm–diameter, 137–mm–long pieces of Type 304 SS bar stock on to each side of an 18.8–mm–diameter, 56–mm–long section of the test material, Fig. 3. The gauge section of the specimens was oriented along the rolling direction for the bar and plate stock. The gauge length of all specimens was given a 1–μm surface finish in the axial direction to prevent circumferential scratches that might act as sites for crack initiation.

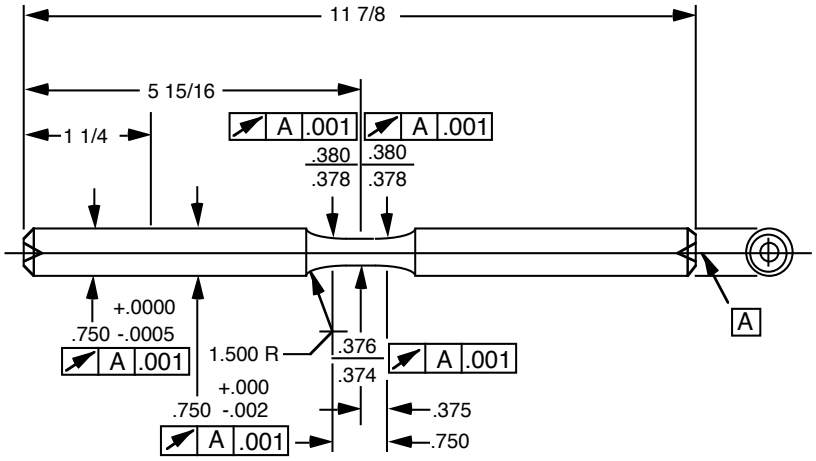

Figure 2. Configuration of fatigue test specimen (all dimensions in inches).

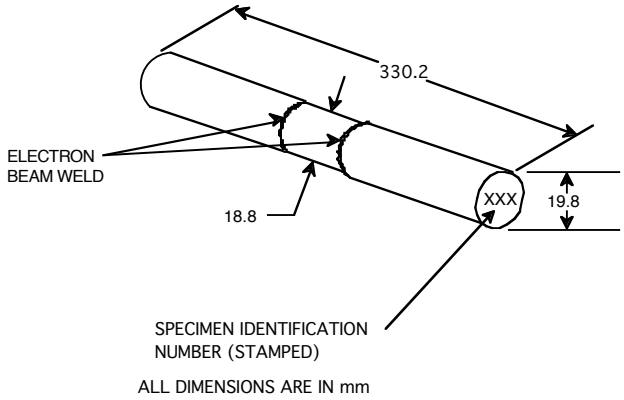

Figure 3. Schematic diagram of electron–beam–welded bar for machining A302–Gr B fatigue test specimens.

Tests in water were conducted in a 12–mL autoclave equipped with a recirculating water system. All tests were conducted at 288°C, with fully reversed axial loading and a triangular or sawtooth waveform. A detailed description of the test facility and test procedures has been presented earlier.[6]

Following testing, ≈10–mm–long sections that contained the fracture surface were cut from the gauge length. These were further stripped of oxides by boiling in a 20 wt.% NaOH and 3 wt.% $KMnO_4$ solution, followed by boiling in a 20 wt.% $(NH_4)_2C_6H_6O_7$ solution. The samples were examined by SEM. Special attention has been paid to crack morphology at the sites of initiation on the fracture surface, and the occurrence of striations. Also, lateral surfaces were inspected to determine the morphology of lateral cracks.

2.3 Results – Effect of Heat Treatment on Fatigue Life

2.3.1 Fatigue ε–N Behavior

Several fatigue tests have been completed on two heats of Type 304 SS under various heat–treatment conditions. These specimens were tested in air and simulated BWR and PWR environments at 289°C. The results from these tests and data obtained earlier on MA Heat 30956 are given in Table 2.

Table 2. Fatigue test results for Type 304 stainless steel in air and simulated BWR and PWR environments at 289°C.

Test No.	Spec. No.	Environ-ment[a]	Dis. Oxygen[b] (ppb)	pH at RT[c]	Conduct-ivity[b] (μS/cm)	ECP Pt[b] mV (SHE)	ECP SS[b] mV (SHE)	Ten. Rate (%/s)	Comp. Rate (%/s)	Stress Amp. (MPa)	Strain Amp. (%)	Life N_{25} (Cycles)
	Heat 30956 MA											
1805	309-03	Air	–	–	–	–	–	4.0E-3	4.0E-1	234.0	0.38	14,410
1853	309-22	BWR	880	6.0	0.06	248	155	4.0E-3	4.0E-1	233.3	0.38	12,300
1856	309-24	BWR	870	6.2	0.07	272	163	4.0E-3	4.0E-1	236.8	0.38	10,450
1808	309-06	PWR	4	6.4	18.87	-693	-690	4.0E-3	4.0E-1	234.2	0.39	2,850
1821	309-09	PWR	2	6.5	22.22	-700	-697	4.0E-3	4.0E-1	237.2	0.38	2,420
1859	309-28	PWR	2	6.5	18.69	-699	-696	4.0E-3	4.0E-1	235.9	0.38	2,420
Heat 30956 MA plus 0.67 h at 700°C												
1893	309-43	Air	–	–	–	–	–	4.0E-3	4.0E-1	236.9	0.38	17,000
1894	309-44	BWR	800	6.7	0.07	263	158	4.0E-3	4.0E-1	239.1	0.38	3,920
1899	309-46	BWR	800	6.2	0.06	285	126	4.0E-3	4.0E-1	241.4	0.38	3,740
1898	309-45	PWR	6	6.3	17.24	-677	-467	4.0E-3	4.0E-1	241.2	0.38	2,530
Heat 30956 MA plus 24 h at 700°C												
1891	309-47	Air	–	–	–	–	–	4.0E-3	4.0E-1	235.8	0.38	16,680
1892	309-48	BWR	860	–	0.06	257	119	4.0E-3	4.0E-1	237.3	0.39	2,790
1897	309-50	PWR	6	6.3	16.67	-629	-543	4.0E-3	4.0E-1	234.1	0.39	2,380
Heat 10285 MA plus 24 h at 600°C												
1895	102-07	Air	–	–	–	–	–	4.0E-3	4.0E-1	222.4	0.38	19,300
1896	102-09	BWR	800	–	0.1	265	206	4.0E-3	4.0E-1	222.2	0.39	1,665
1900	102-08	PWR	7	6.2	16.95	-522	-527	4.0E-3	4.0E-1	228.0	0.37	2,840

[a]PWR = simulated PWR water with 2 ppm Li, 1000 ppm B, and ≈2 ppm dissolved H_2 (or ≈23 cc/kg) in the feedwater;
BWR = high-purity deionized water.
[b]Measured in effluent.
[c]RT = room temperature.

The effect of heat treatment on the fatigue life of Type 304 SS in air, BWR, and PWR environments is shown in Fig. 4. Fatigue life is plotted as a function of the EPR value for the various material conditions. The results indicate that heat treatment has little or no effect on the fatigue life of Type 304 SS in air and PWR environments. In a BWR environment, fatigue life is lower for the sensitized SSs. The decrease in life seems to increase with increasing EPR value.

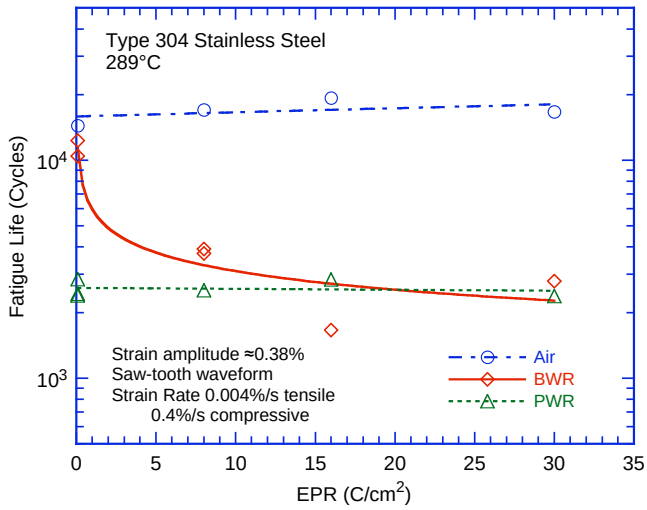

Figure 4.
Effect of material heat treatment on fatigue life of Type 304 stainless steel in air, BWR, and PWR environments at 289°C, ≈0.38% strain amplitude, sawtooth waveform, and 0.004%/s tensile strain rate.

These results are consistent with the data obtained at Mitsubishi Heavy Industries, Ltd. (MHI)[10–12] and Ishikawajima–Harima Heavy Industries Co. (IHI)[13] on solution–annealed and sensitized Type 304, 316, and 316NG SS (Figs. 5 and 6). For example, in low–DO (<0.005 ppm) water, environmental effects on the fatigue life of Type 304 and 316 SS are significant irrespective of material heat treatment (Fig. 5). In high–DO (8 ppm) water, the fatigue life of solution–annealed Type 304 SS is a factor of ≈2 longer than that of the sensitized steel (Fig 6a). A sensitization anneal appears to have little or no effect on the fatigue life of Type 316NG SS in high–DO water at 288°C (Fig. 6b). Fatigue lives of solution–annealed and sensitized Type 316NG SS are comparable.

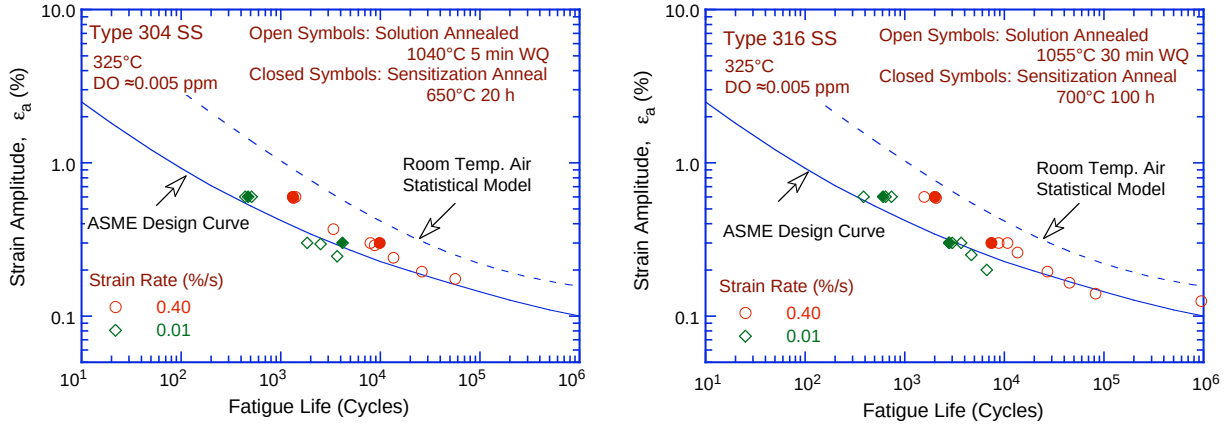

(a) (b)

Figure 5. Effect of sensitization annealing on fatigue life of Type (a) 304 and (b) 316 stainless steel in low–DO water at 325°C (Refs. 10,11). WQ = water quenched.

The cyclic stress response of the various materials in air, BWR, and PWR environments at 289°C is shown in Fig. 7. As expected, the cyclic strain–hardening behavior of Type 304 SS under various heat treatment conditions is identical; only the fatigue life varies in the environments.

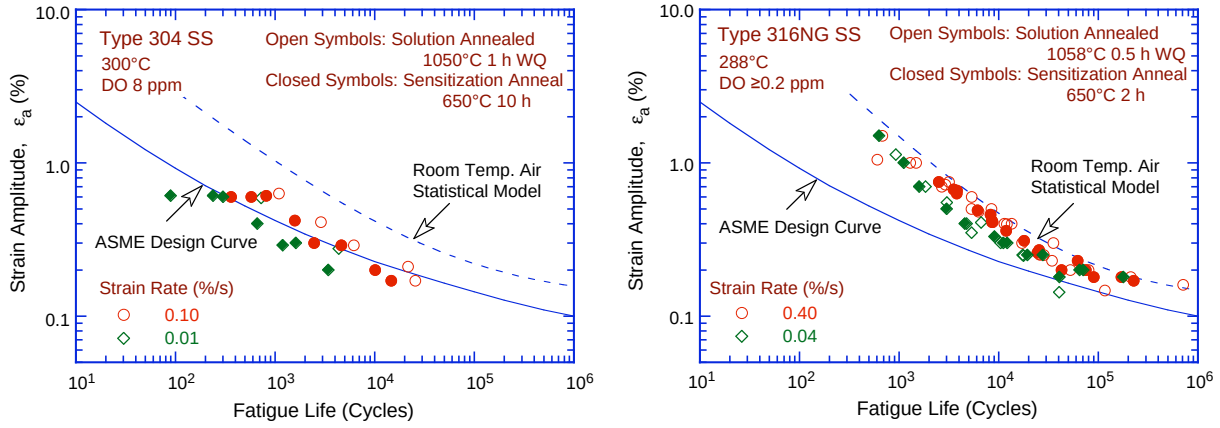

Figure 6. Effect of sensitization anneal on the fatigue lives of Type (a) 304 and (b) 316NG stainless steel in high–DO water (Refs. 12,13). WQ = water quenched.

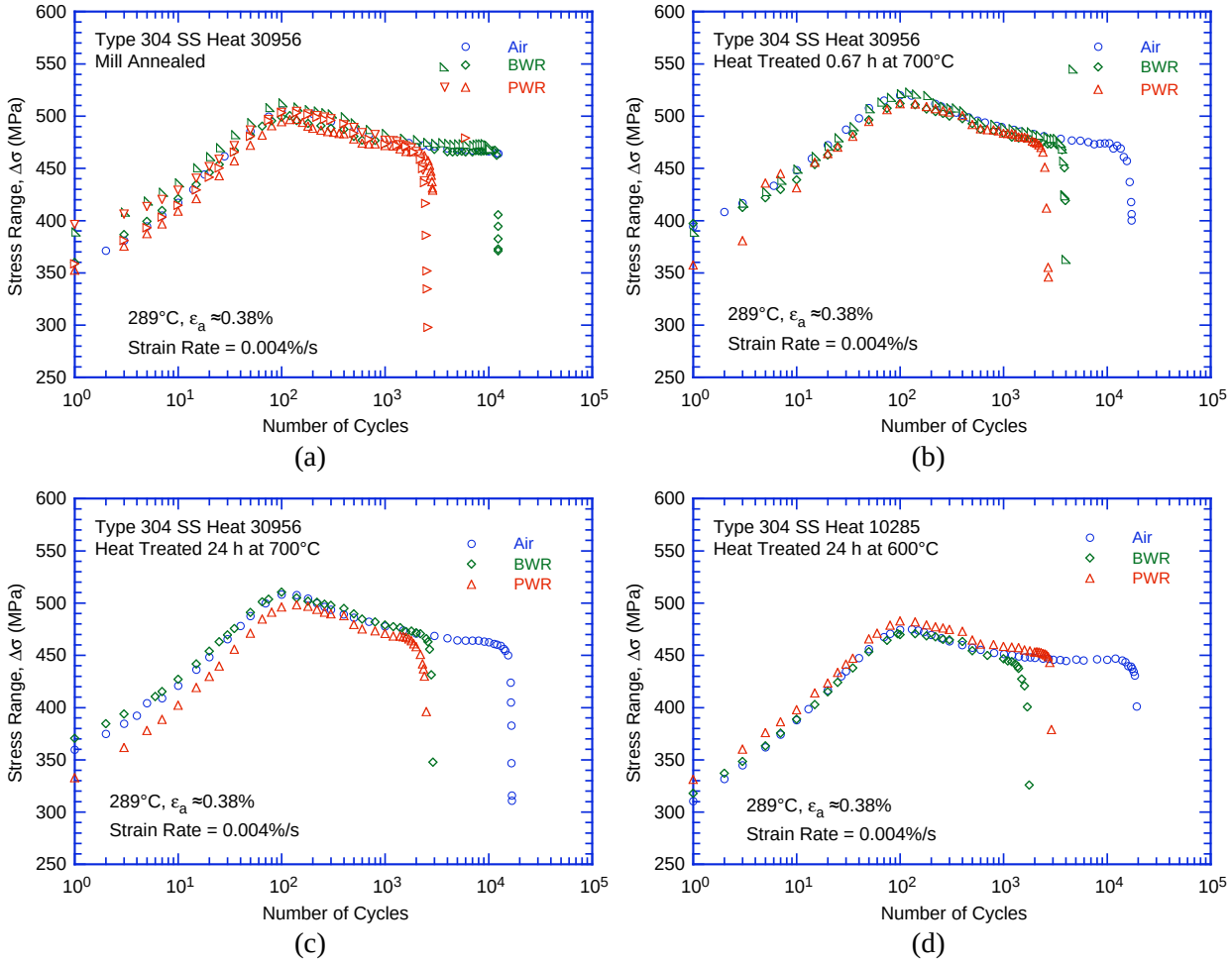

Figure 7. Cyclic stress response of Heat 30956: (a) MA, (b) MA + 0.67 h at 700°C, and (c) MA + 24 h at 700°C; and Heat 10285, (d) MA + 24 h at 600°C in air, BWR, and PWR environments at 289°C.

2.3.2 Fatigue Crack and Fracture Surface Morphology

A detailed metallographic evaluation of the fatigue test specimens was performed to characterize the crack and fracture morphology of the various heats under different heat treatment conditions. Figure 8 shows low– and high–magnification crack initiation sites on the fracture surfaces of the sensitized Type 304 SS tested in air. Apparently, irrespective of the degree of sensitization, the fracture mode for crack initiation (i.e., crack lengths up to ≈200 μm) and crack propagation (i.e., crack lengths >200 μm) is transgranular (TG), most likely along crystallographic planes, leaving behind relatively smooth facets. With increasing degree of sensitization, cleavage–like or stepped TG fracture (e.g., Figs. 8 c and d), and occasionally ridge structures were observed on the smooth surfaces (e.g., Figs. 8e and f).

The effect of a simulated normal–water chemistry BWR environment, Fig. 9, was to cause intergranular (IG) crack initiation, implying a weakening of the grain boundaries. In the BWR environment, the initial crack appeared IG under all heat–treated conditions. Photomicrographs of the fracture surface of the more heavily sensitized steel, e.g., Heat 30956 MA + 24 h at 700°C (Figs. 9g and h) and especially Heat 10285 MA + 24 h at 600°C (Figs. 9e and f), are good examples of smooth IG fracture. Furthermore, comparison of the four material conditions indicates that the extent of IG fracture increases with the degree of sensitization, at least through the MA + 24 h at 600°C condition, whereas MA + 24 h at 700°C appears to have a somewhat more mixed IG and TG morphology. Also, one effect of the BWR environment (Figs. 9a–h) was to cause IG crack initiation, implying a weakening of the grain boundaries. Nevertheless, for all four conditions tested, the initial IG mode transformed within <200 μm into a TG mode with cleavage–like features. By contrast, for all samples of Type 304 SS tested in PWR environments (Fig. 10), cracks initiated and propagated in a TG mode irrespective of the degree of sensitization. Prominent features of all fracture surfaces are highly angular, cleavage–like facets that exhibit well–defined "river" patterns. Intergranular facets were rare, mostly in the more heavily sensitized alloys. These observations suggest brittle behavior throughout the testing period.

Fatigue striations normal to the crack advance direction were clearly visible beyond ≈200 μm on the fracture surfaces of all materials under all environmental conditions, as documented in Figs. 11–14. For example, for the MA Heat 30956 samples tested in BWR water (Fig. 11), striations were easily discernible on the facets irrespective of the steps, cleavage–like features, or river patterns. Similar striations were also observed on the fracture surface of MA Heat 30956 heat–treated 0.67 h at 700°C irrespective of the testing environment (Fig. 12). Striations were found on both the TG and IG facets of the samples tested under BWR conditions, or co-existing with the "river" patterns specific to the samples tested in the PWR environment. Evidence of extensive rubbing due to repeated contact between the two mating surfaces (Figs. 12a and b) was also found.

Figure 13 shows fatigue striations observed on the fracture surface of MA Heat 10285 heat–treated 24 h at 600°C. In spite of the wide coverage with rubbing and fretting marks, striations are clearly observed on some facets. Figures 13e and f show striations on one IG facet in a sample tested in PWR conditions. The fracture surfaces of MA Heat 30956 heat–treated 24 h at 700°C are presented in Fig. 14. Low– and high–magnification photomicrographs are presented of fatigue striations on faceted, stepped TG, and cleavage–like fracture surfaces.

Air Environment

Heat 30956 mill annealed plus heat treated 0.67 h at 700°C

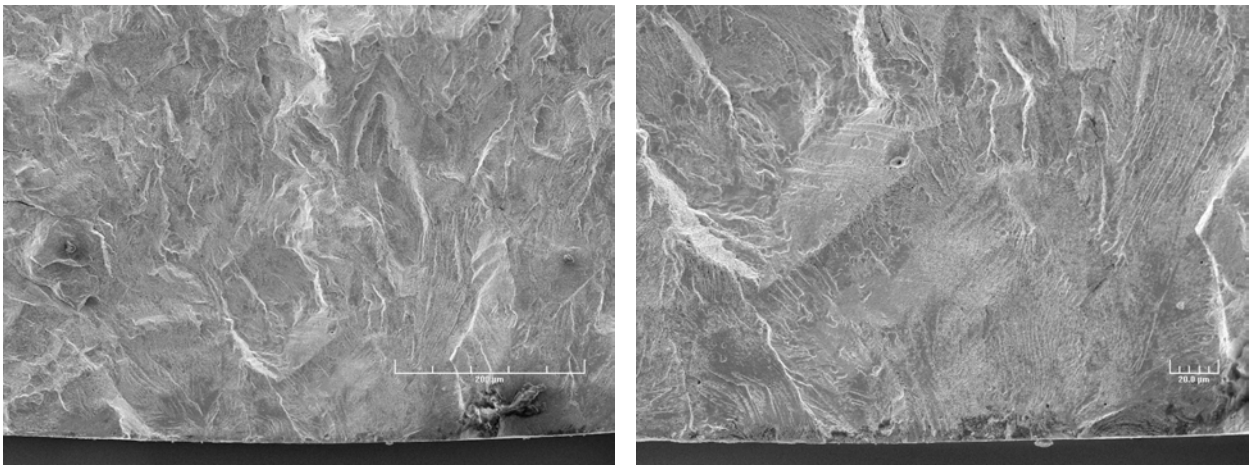

(a) (b)

Heat 10285 mill annealed plus heat treated 24 h at 600°C

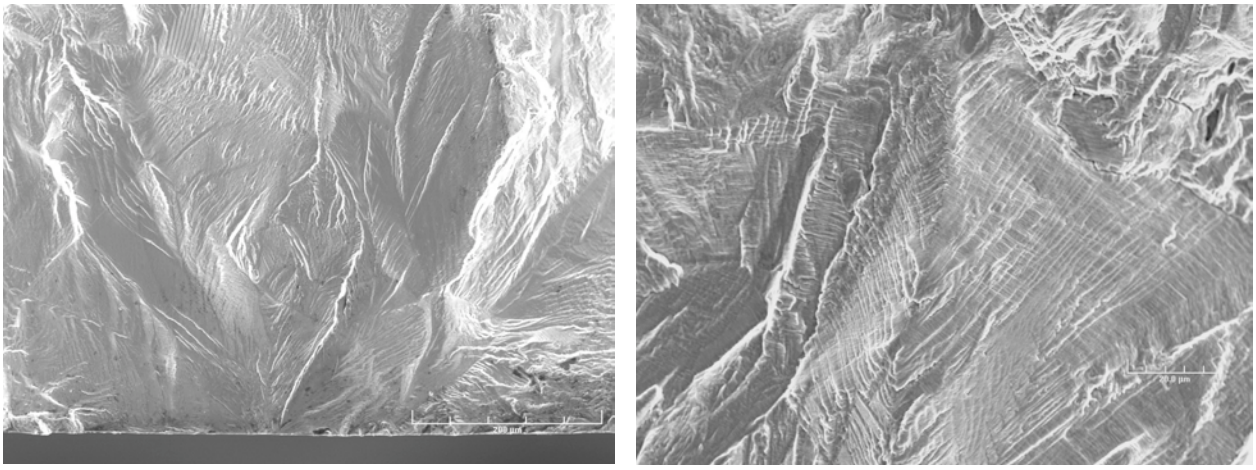

(c) (d)

Heat 30956 mill annealed plus heat treated 24 h at 700°C

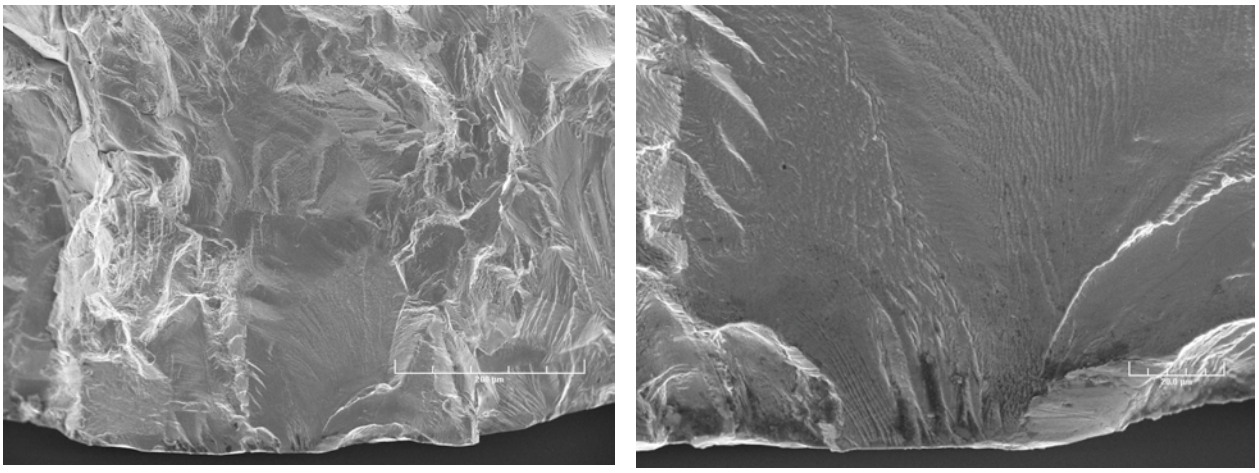

(e) (f)

Figure 8. Photomicrographs showing sites of crack initiation on fracture surfaces of Type 304 SS specimens tested in air: (a), (c), (e), low magnification; (b), (d), (f), high magnification.

Simulated BWR Environment

Heat 30956 mill annealed

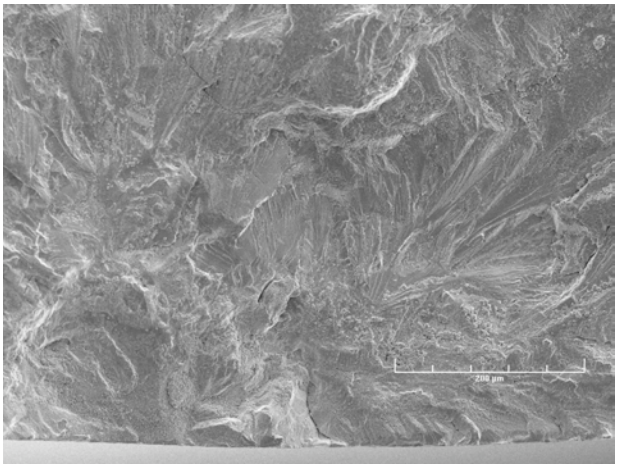

(a)

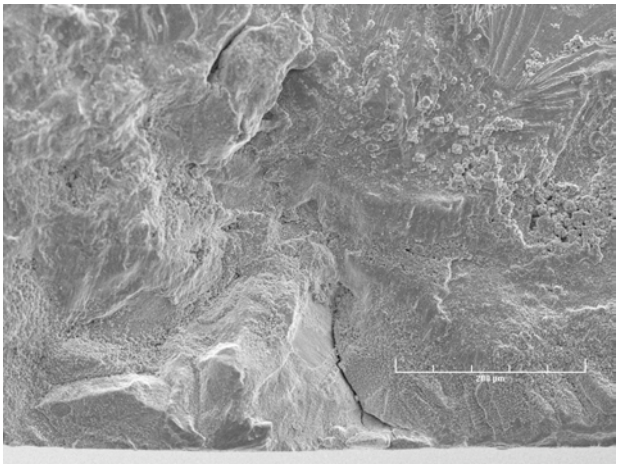

(b)

Heat 30956 mill annealed plus heat treated 0.67 h at 700°C

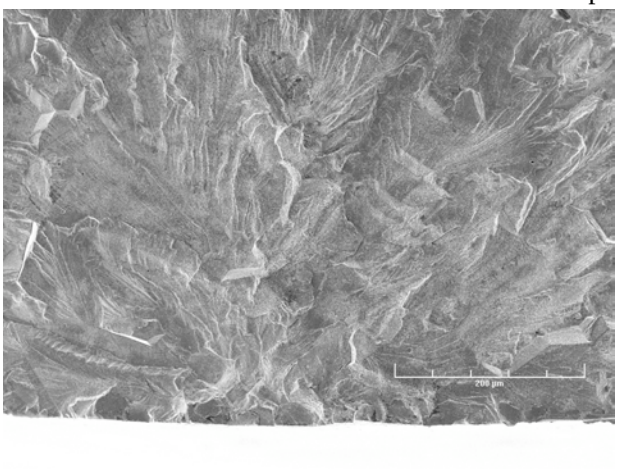

(c)

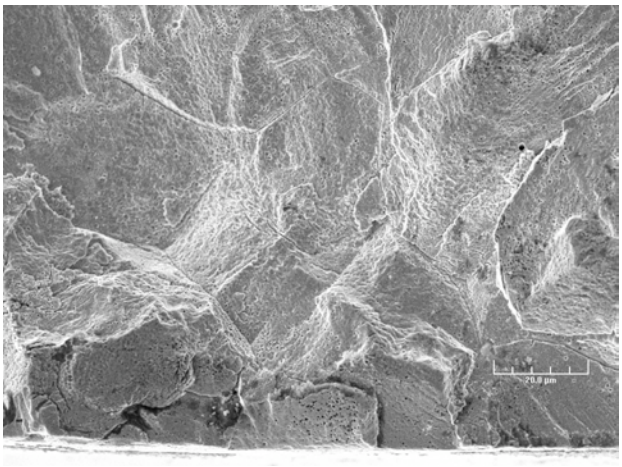

(d)

Heat 10285 mill annealed plus heat treated 24 h at 600°C

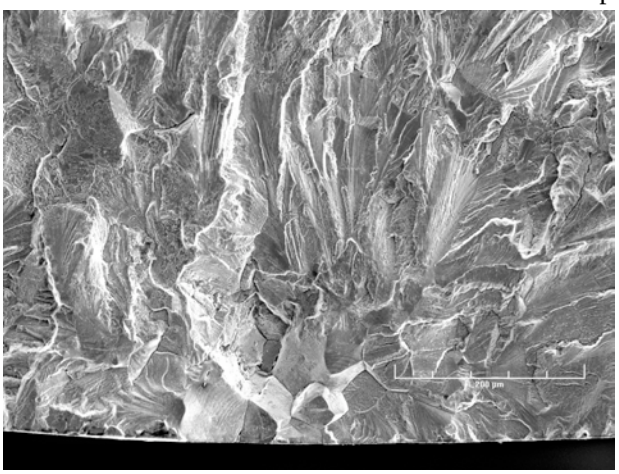

(e)

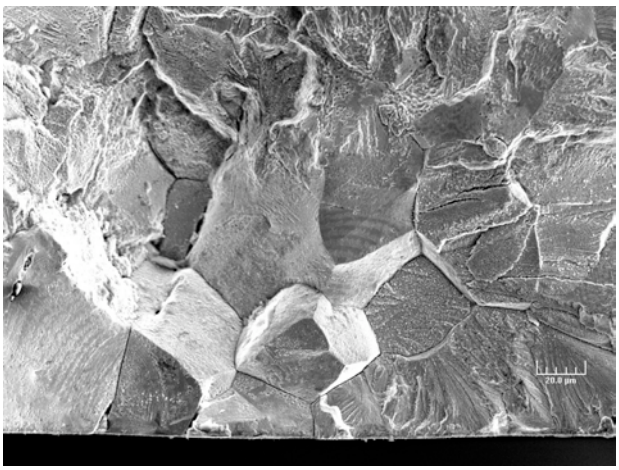

(f)

Heat 30956 mill annealed plus heat treated 24 h at 700°C

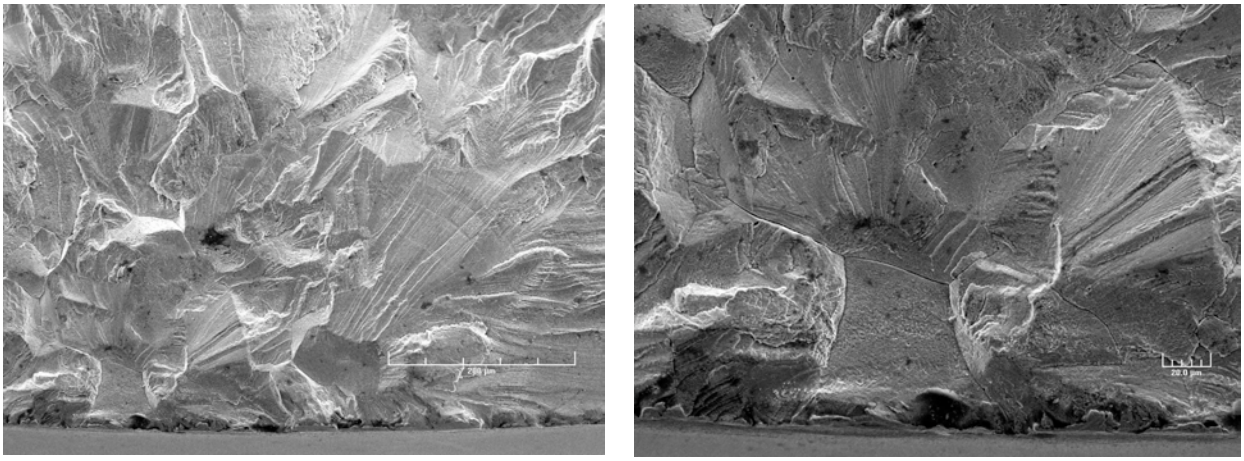

(g) (h)

Figure 9. Photomicrographs showing sites of crack initiation on fracture surfaces of Type 304 SS specimens tested in simulated BWR environment: (a), (c), (e), (g) low magnification; (b), (d), (f), (h) high magnification.

Simulated PWR Environment

Heat 30956 mill annealed

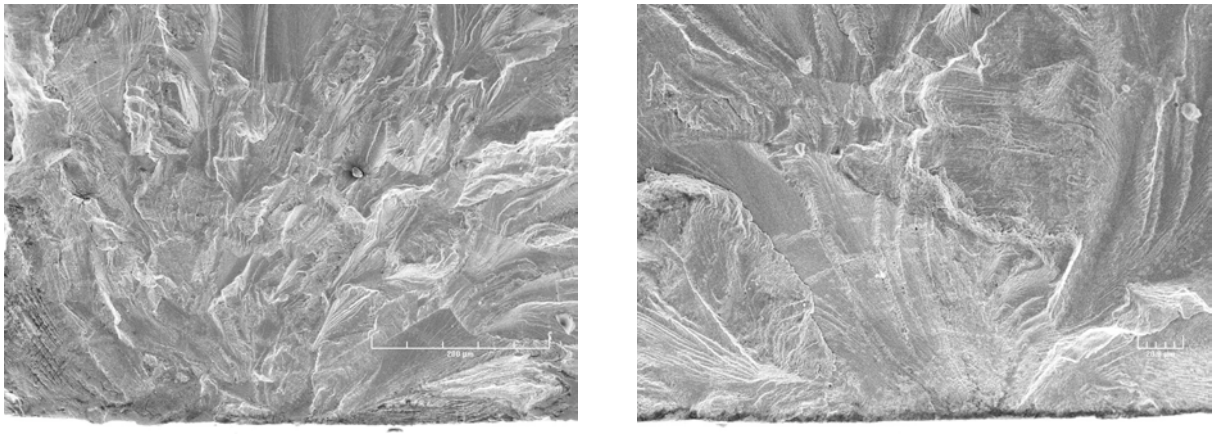

(a) (b)

Heat 30956 mill annealed plus 0.67 h at 700°C

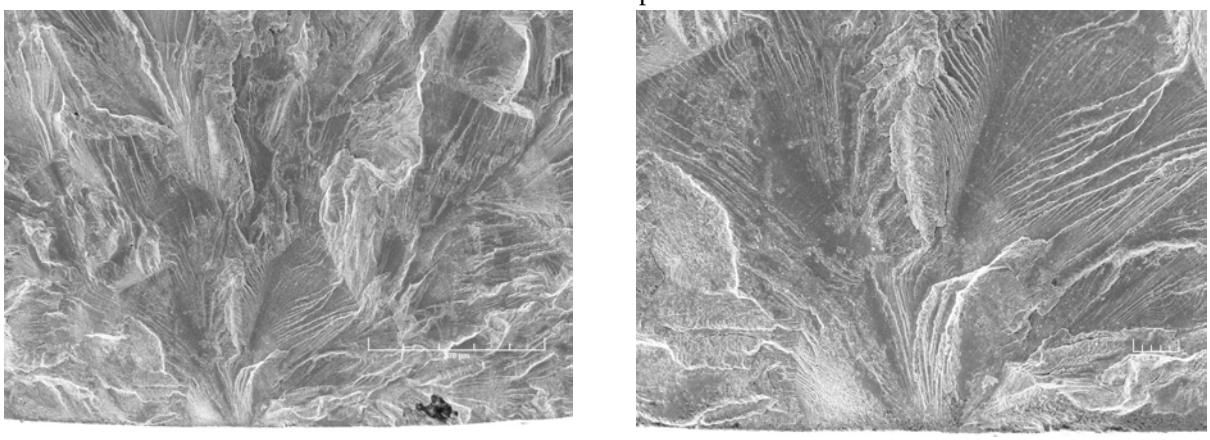

(c) (d)

Heat 10285 mill annealed plus 24 h at 600°C

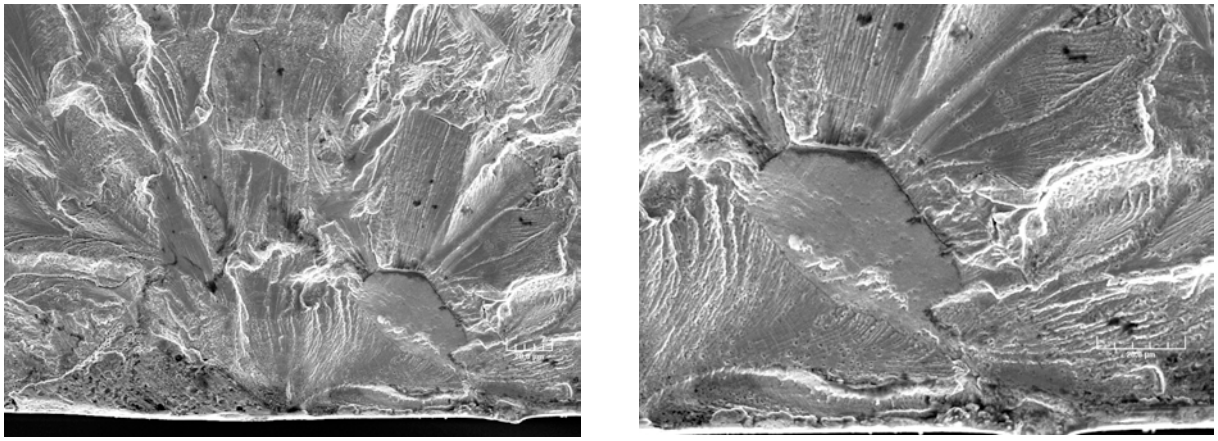

(e) (f)

Heat 30956 mill annealed plus 24 h at 700°C

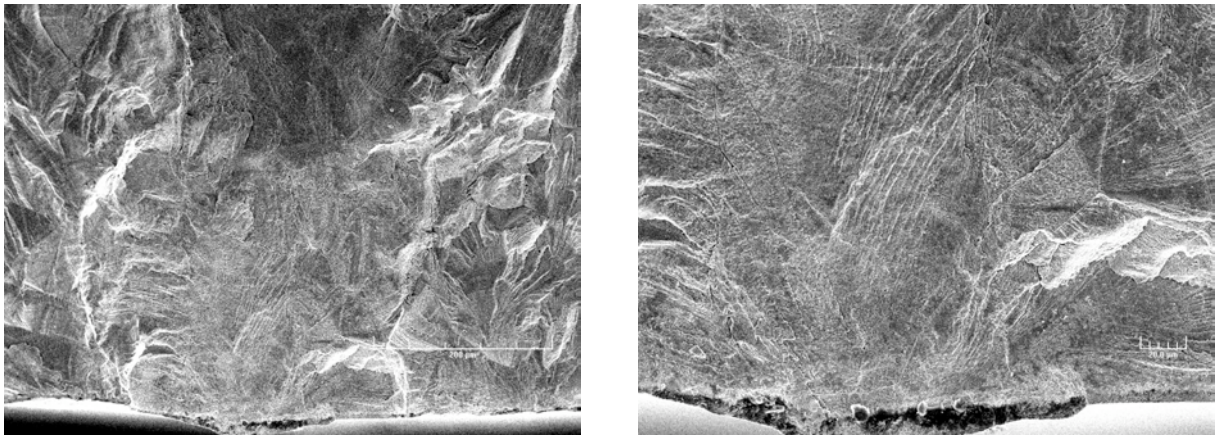

(g) (h)

Figure 10. Photomicrographs showing the sites of crack initiation on the fracture surfaces of Type 304 SS specimen tested in simulated PWR environment: (a), (c), (e), (g) low magnification; (b), (d), (f), (h) high magnification.

Simulated BWR environment

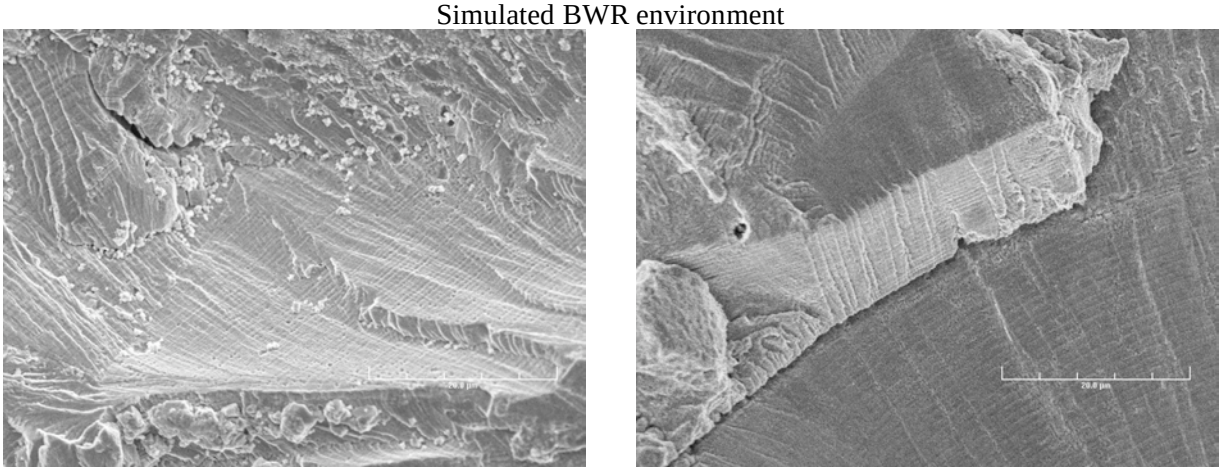

(a) (b)

Figure 11. (a) Low– and (b) high–magnification photomicrographs showing striations at select locations on fracture surfaces of MA specimen of Heat 30956 in simulated BWR environment.

Heat 30956 mill annealed plus 0.67 h at 700°C

Air Environment

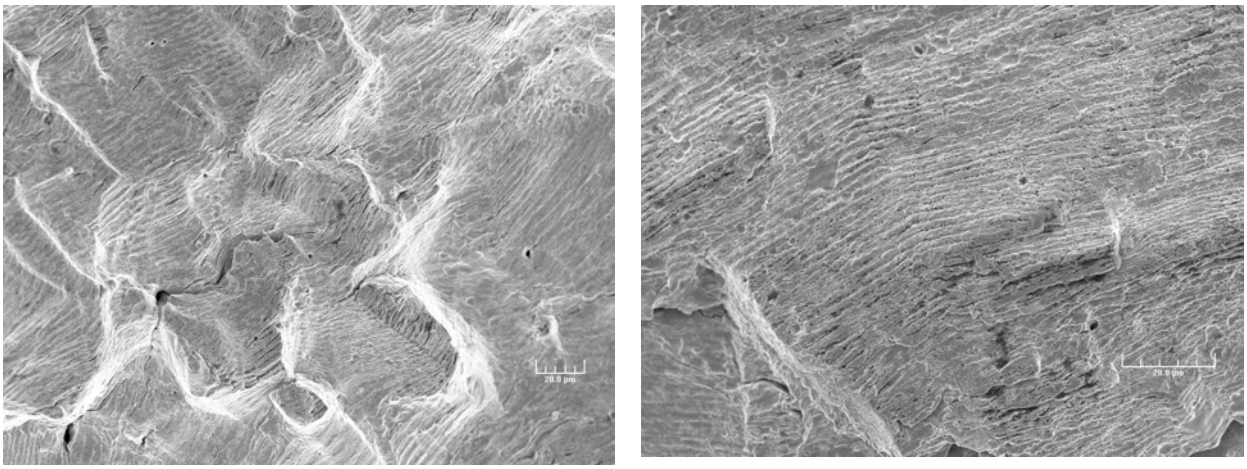

(a) (b)

Simulated BWR Environment

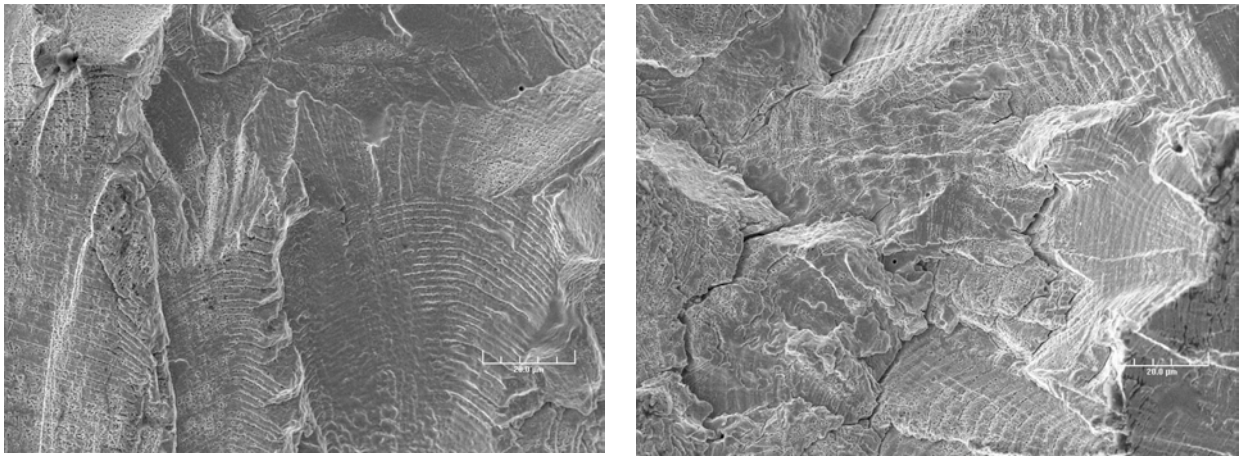

(c) (d)

Simulated PWR Environment

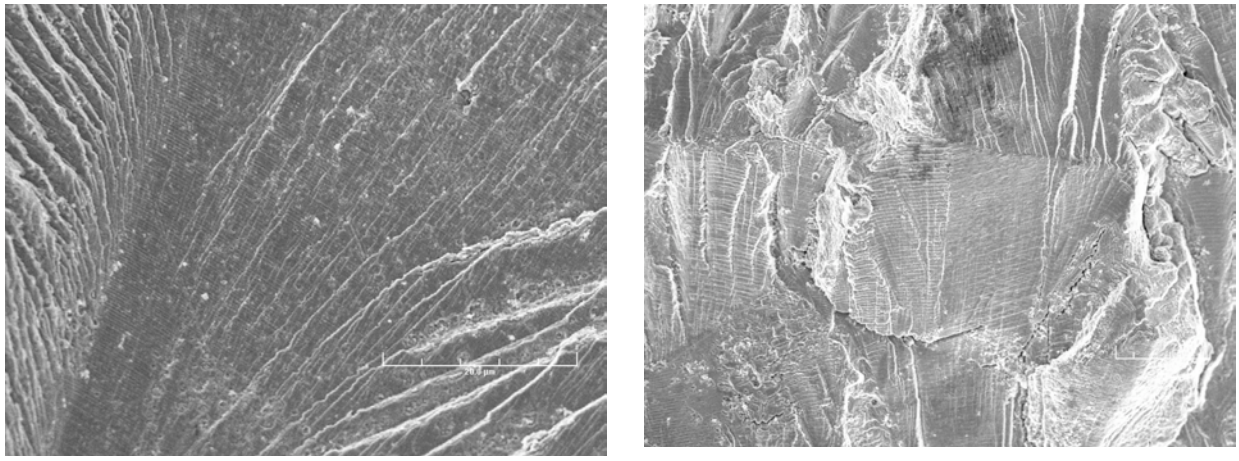

(e) (f)

Figure 12. Photomicrographs showing striations at select locations on fracture surfaces of MA specimens of Heat 30956 heat–treated for 0.67 h at 700°C in air, BWR, and PWR environments: (a), (c), (e) low magnification; (b), (d), (f) high–magnification.

Heat 10285 mill annealed plus 24 h at 600°C

Air Environment

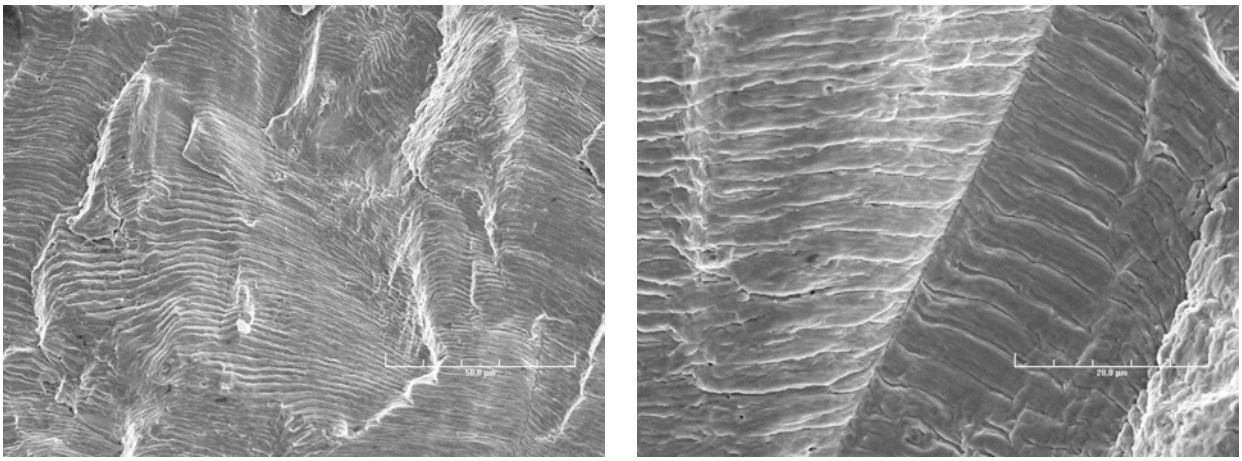

(a) (b)

Simulated BWR Environment

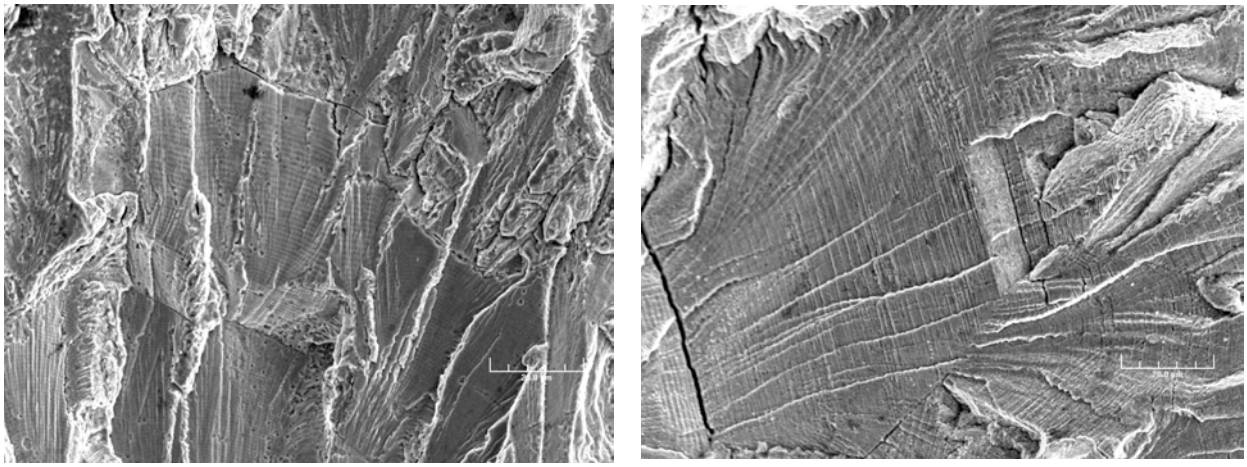

(c) (d)

Simulated PWR Environment

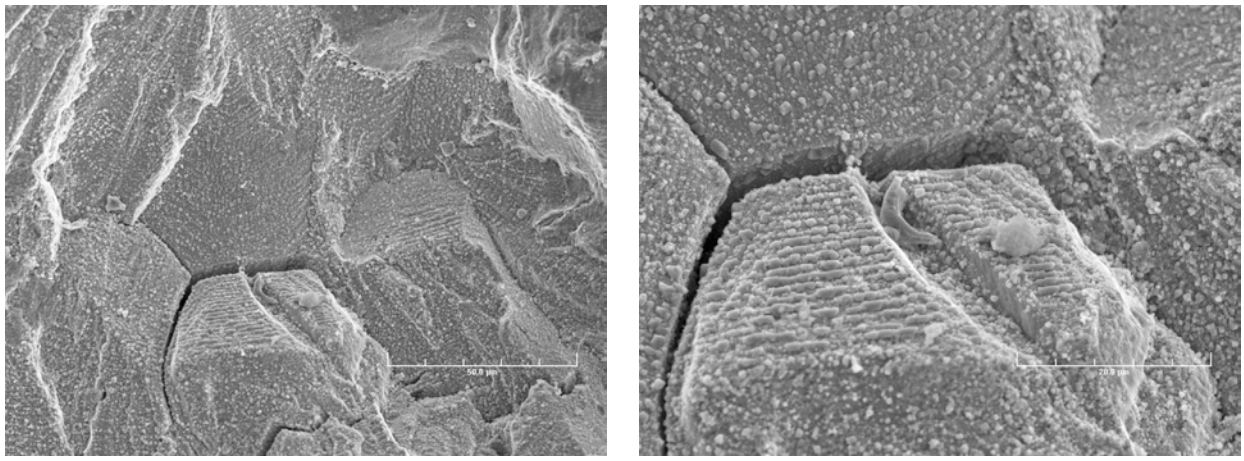

(e) (f)

Figure 13. Photomicrographs showing striations at select locations on fracture surfaces of MA specimens of Heat 10285 heat–treated for 24 h at 600°C in air, BWR, and PWR environments: (a), (c), (e) low magnification; (b), (d), (f) high–magnification.

Heat 30956 mill annealed plus 24 h at 700°C

Air Environment

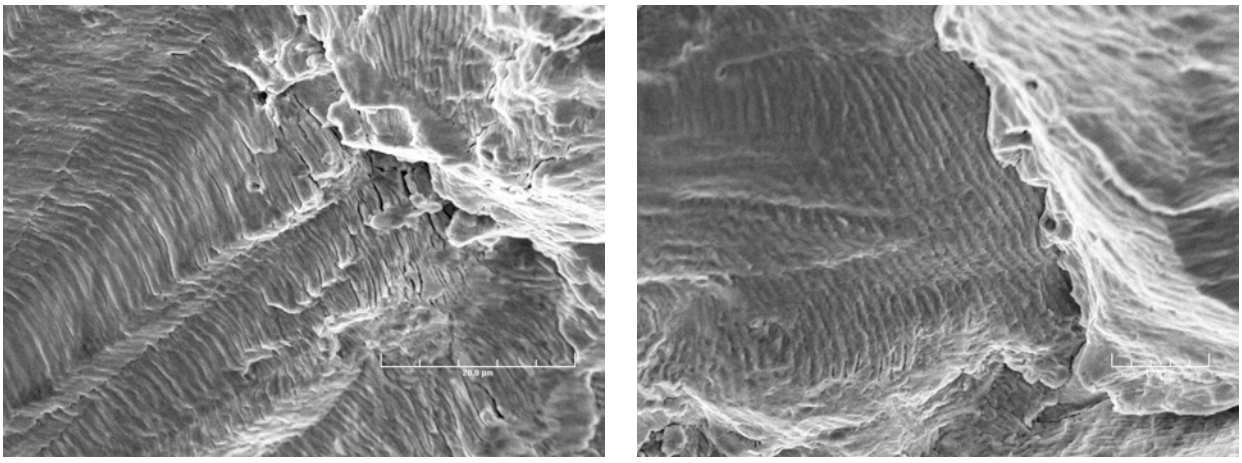

(a) (b)

Simulated BWR Environment

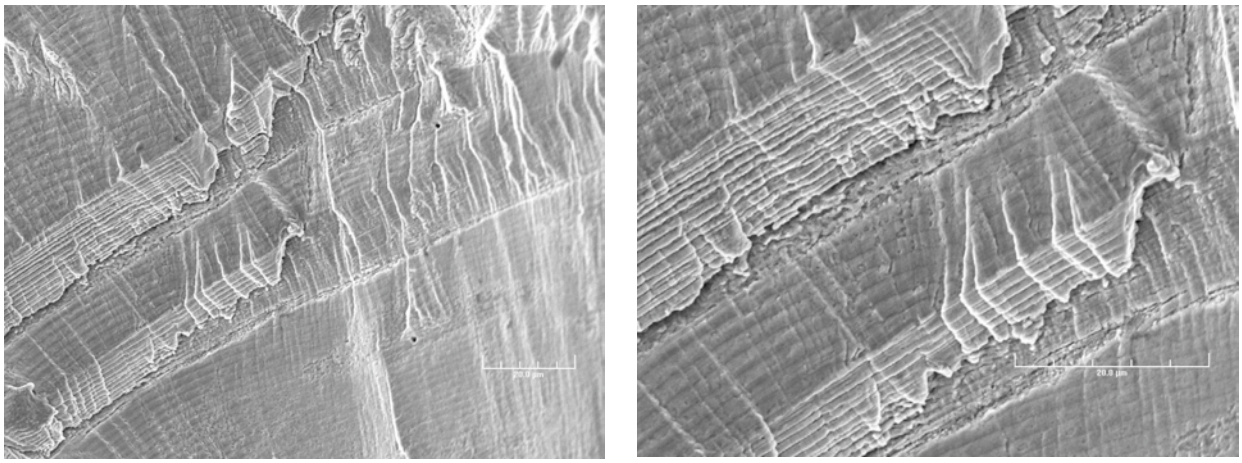

(c) (d)

Simulated PWR Environment

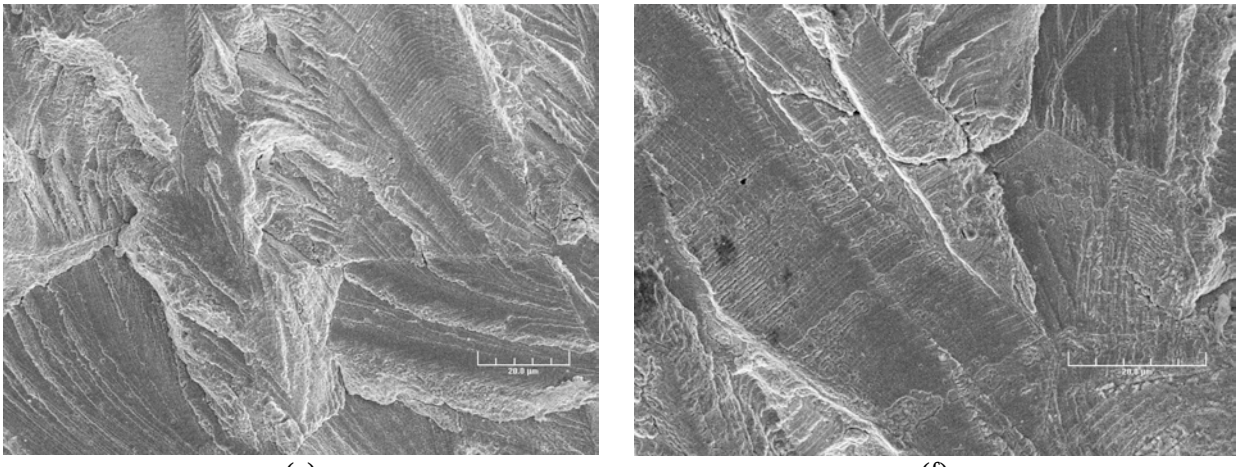

(e) (f)

Figure 14. Photomicrographs showing striations at select locations on fracture surfaces of MA specimens of Heat 30956 heat–treated for 24 h at 700°C in air, BWR, and PWR environments: (a), (c), (e) low magnification; (b), (d), (f) high–magnification.

Photomicrographs of the crack morphology of Type 304 SS under all test and environmental conditions are presented in Fig. 15. In all cases, the tensile axis is vertical and parallel to the plane of each picture. In general, for air tests the cracks are more likely to be oblique, approaching 45° with respect to the tensile axis. By contrast, the cracks that form in either BWR or PWR environments tend to be perpendicular to the tensile axis.

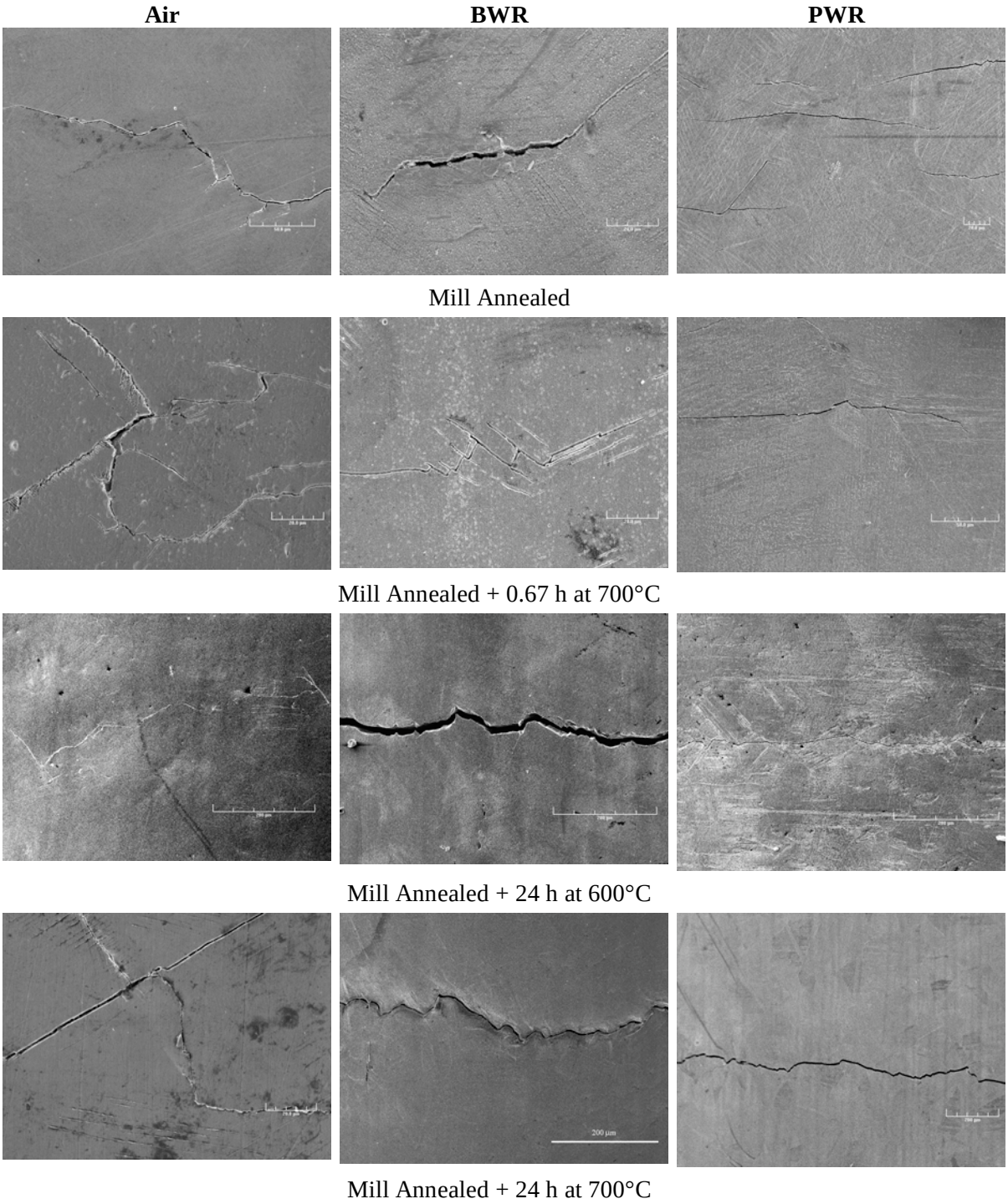

Figure 15. Photomicrographs of the crack morphology of Type 304 SS under all test and environmental conditions.

The metallographic evaluations of the fatigue test specimens may be summarized as follows. In air, cracking was initiated as TG, oblique with respect to the tensile axis. In BWR environments, cracking was initiated as IG, normal to the tensile axis. By contrast, in PWR environments cracking was initiated as TG, but still normal to the tensile axis. Cracking propagated as TG irrespective of the environment.

The crack and fracture morphology in Type 316NG SS specimens (Heat D432804) from earlier tests was also evaluated for comparison. Figure 16 shows, at low and high magnification, crack initiation sites on the fracture surfaces of Type 316NG specimens tested in air. Note that the cracks were initiated and propagated in the TG mode, most likely along crystallographic planes, leaving behind highly angular, cleavage–like or stepped surface features. Figures 16c and d show striations on some highly angular facets.

In a high–DO BWR environment, Fig. 17a–c, cracking was also initiated and propagated in TG mode, with riverlike patterns on the facets. Within 200 μm of the initiation site, fatigue striations were observed on some facets (Figs. 17b and c). Similarly, for specimens tested in a low–DO PWR environment (Fig. 17d), crack initiation and crack propagation are TG, with cleavage–like fracture facets

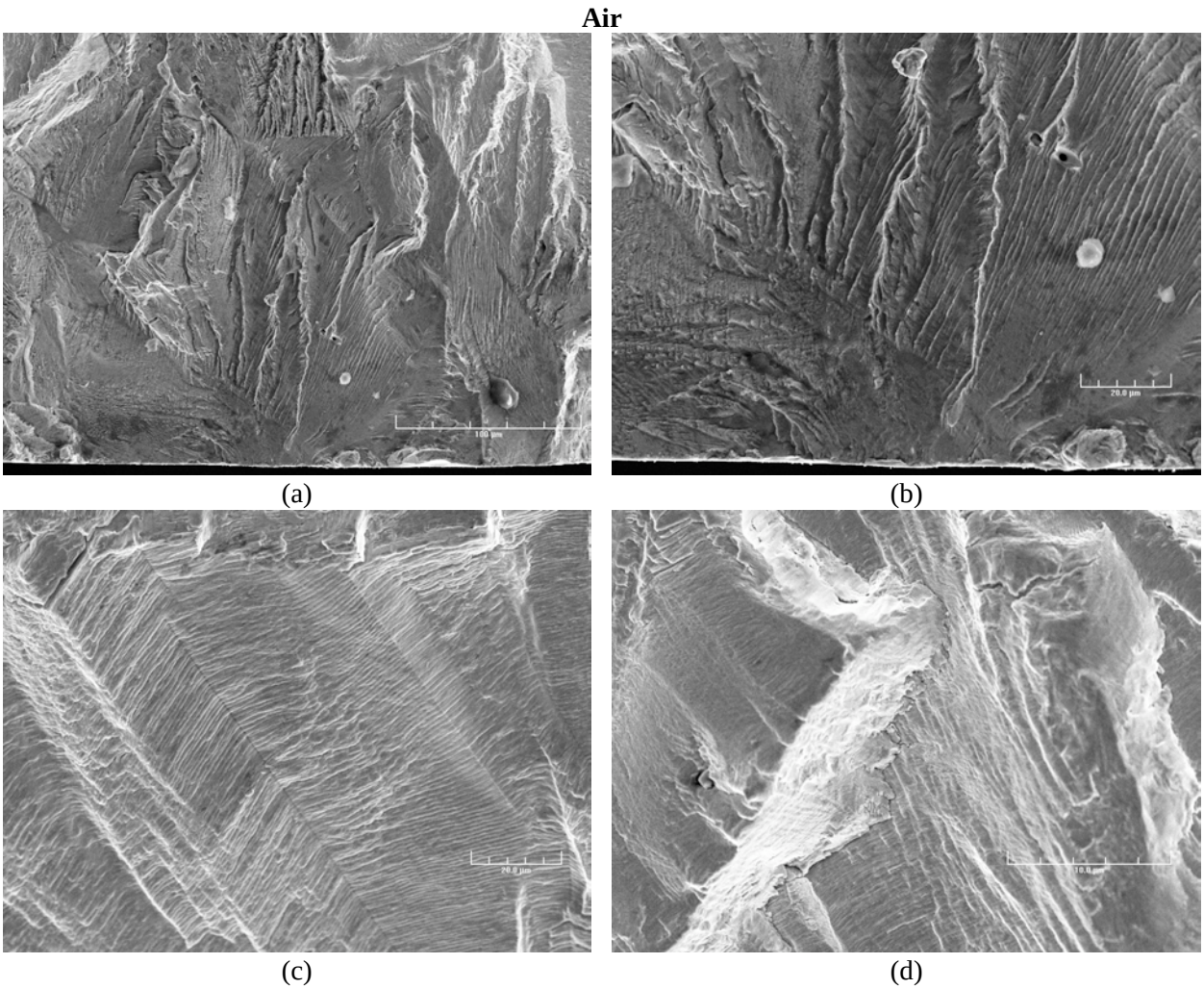

Figure 16. Photomicrographs showing crack initiation site at (a) low and (b) high magnification, and (c,d) striations at select locations in Type 316NG SS tested in air.

that exhibit river patterns. The higher magnification photomicrographs (at a location seen in Fig. 17d) show fatigue striations within 200 μm of the initiation site. Evidence of rubbing due to repeated contact between the two mating surfaces can also be observed in Fig. 17f.

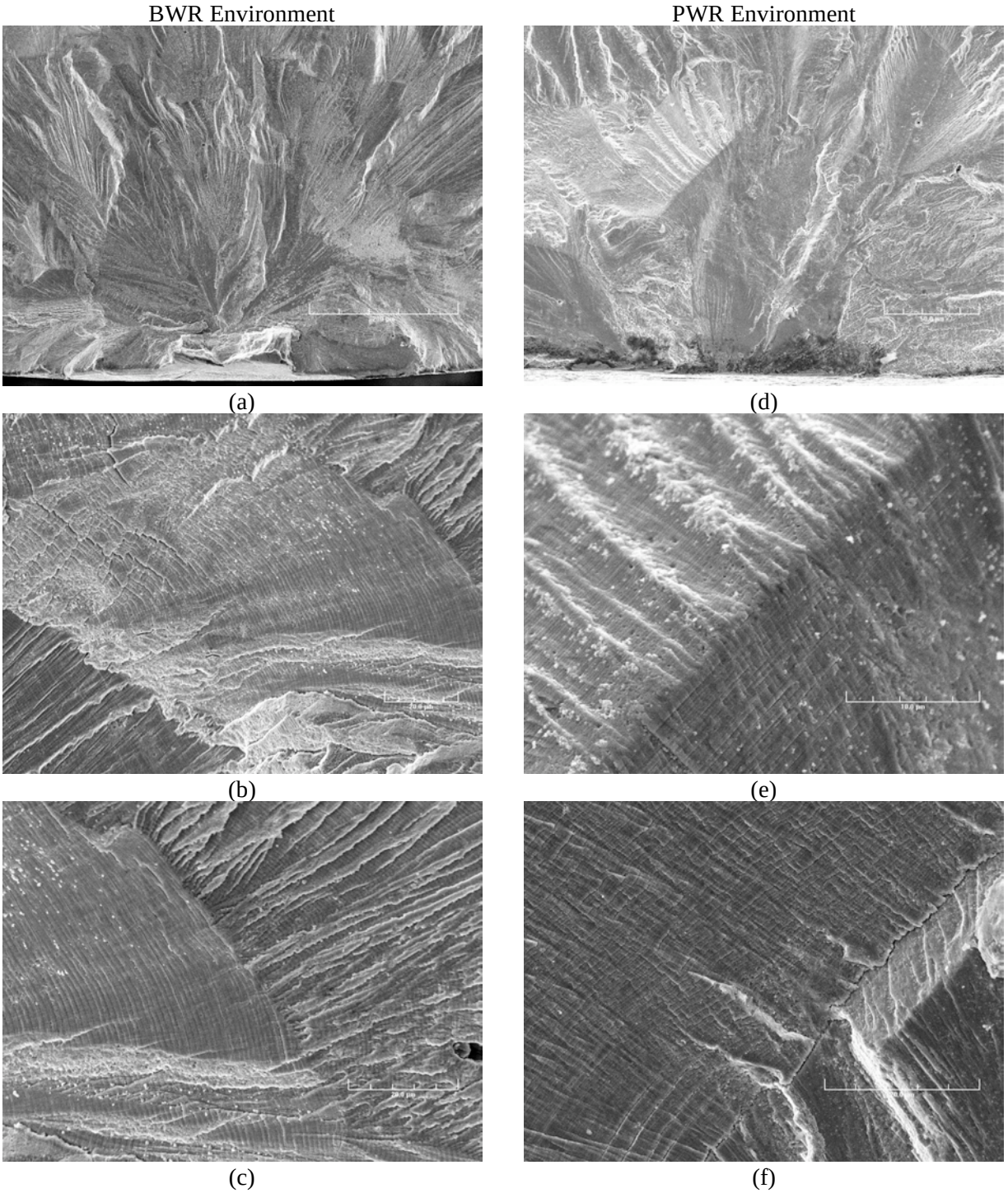

Figure 17. Photomicrographs showing crack initiation site and striations at select locations in Type 316NG SS tested in (a–c) BWR and (d–f) PWR environment.

Figure 18 presents photomicrographs that show the crack morphology in Type 316NG SS in three environments. In all cases, the tensile axis is vertical, parallel to the plane of each picture. The general appearance is that, for air tests, the cracks are more likely to be oblique, approaching 45° with respect to the tensile axis. By contrast, the cracks that formed in the BWR environment appeared mixed, both oblique and normal to the tensile direction, while the cracks that formed in the PWR environment appeared mostly perpendicular to the tensile axis.

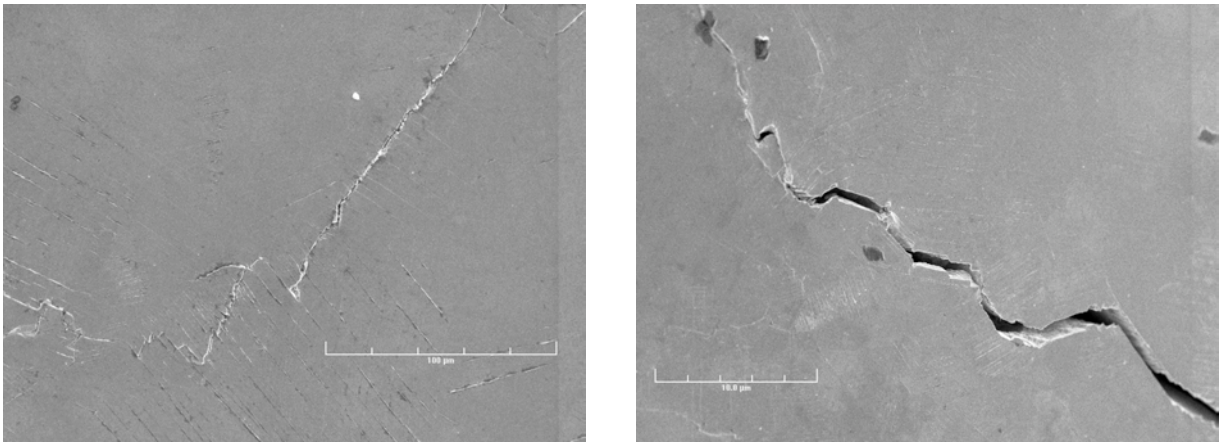

Air

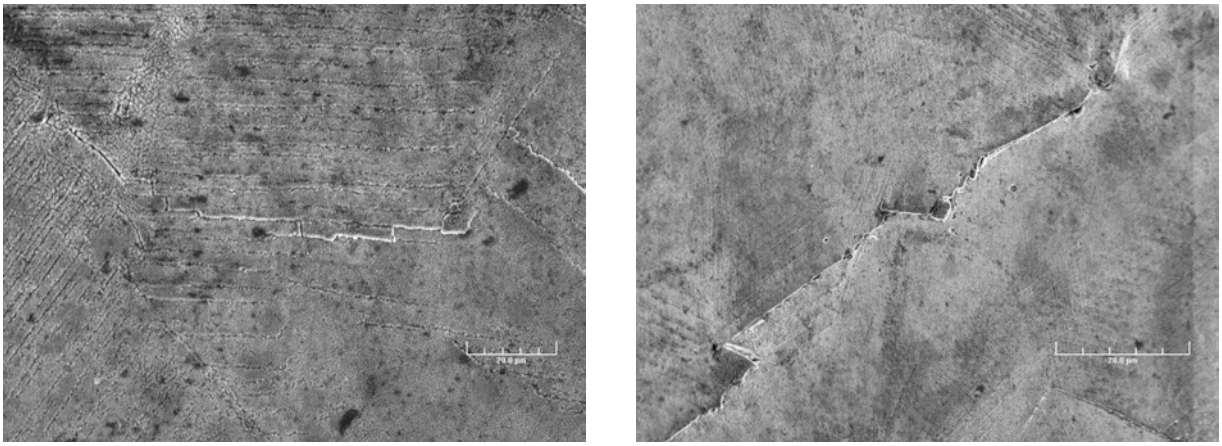

BWR Environment

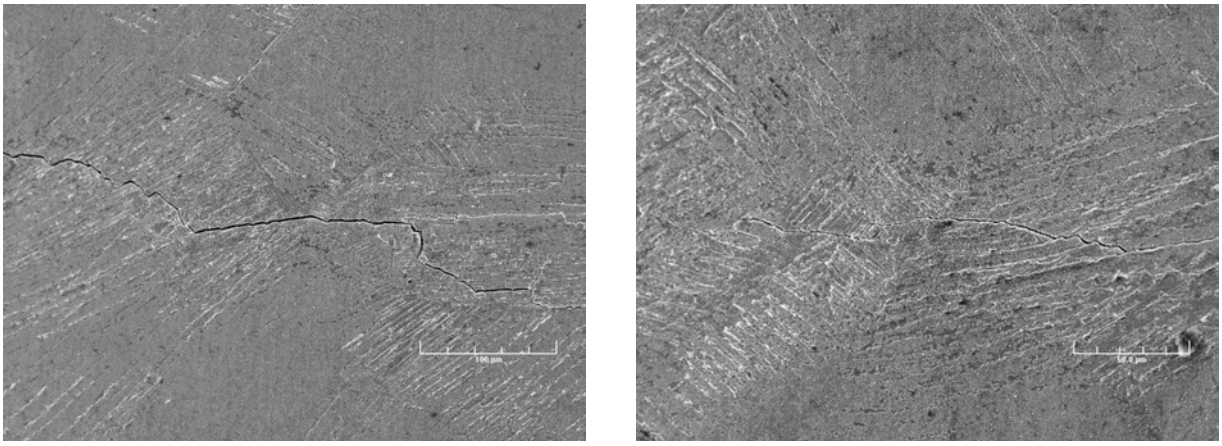

PWR Environment

Figure 18. Photomicrographs showing the morphology of lateral cracks formed in Type 316NG SS in three test environments.